Communication

Received: 31 July 2025 Revised: 28 October 2025 Published online in Wiley Online Library:

(wileyonlinelibrary.com) DOI 10.1002/pi.70054

Impact of polymer aging on main-chain poly(fullerene)s with halide chain-ends for inverted perovskite solar cells

João V. Paulin,[a] Gabriel L. Nogueira,[a] Douglas H. N. Santos,[b] Marco Antônio G. B. Gomes,[c] Valdemiro P. Carvalho-Jr,[b] Luiz C. Silva Filho,[d] Roger C. Hiorns[c*] and Carlos F. O. Graeff[a*]

Abstract

As perovskite solar cells (PSCs) advance toward commercialization, the need for stable and easily processable materials becomes increasingly important. In this study, we examine how the aging of polymeric electron transport layers (ETLs) affects the performance of inverted PSCs. Two main-chain poly(fullerene)s, $PC_{60}DB_{(IMP)}$ and $PC_{60}DB_{(ATRAP)}$, which differ only in their terminal halogen groups, were stored under nitrogen, in the dark and at room temperature, for up to 11 months before device fabrication. Devices using aged $PC_{60}DB_{(IMP)}$ showed significant drops in efficiency, while those based on $PC_{60}DB_{(ATRAP)}$ maintained more stable performance and even exhibited reduced hysteresis over time. These contrasting results appear to stem from differences in halogen reactivity, with iodine likely triggering degradation pathways not seen in the bromine-containing counterpart. Altogether, the findings highlight how thoughtful molecular design can improve the long-term stability and practical use of ETL materials in scalable PSC technologies.

Supporting information may be found in the online version of this article.

Keywords: electron transport layer; perovskite solar cells; poly(fullerene)s; polymers; stability

INTRODUCTION

The growing concern over climate change has brought urgent attention to the need for cleaner and sustainable energy sources. Global efforts to reduce carbon emissions have pushed the scientific community to explore alternatives to fossil fuels.[1] Among various renewable technologies, solar energy stands out due to its abundance and accessibility.[1] However, to fully realize its potential, the development of efficient, low-cost and scalable photovoltaic materials remains a key challenge.[1,2]

In this context, the perovskite solar cell (PSC) has emerged as one of the most promising technologies. Its rapid progress in power conversion efficiency, combined with relatively simple and relatively low-cost fabrication processes, has attracted significant interest in both academic and industrial settings.

A typical PSC consists of multiple functional layers that work together to absorb light, separate charges and transport them to the electrodes.[1–4] Their layered architecture allows for versatile design and fine-tuning of interfacial processes, which are essential for both device performance and long-term stability. In particular, interfacial transport layers are especially critical. For instance, the electron transport layer (ETL) must efficiently collect photogenerated electrons and block holes to minimize recombination losses.[1–4]

To fulfill these functions, several materials have been explored, with fullerene-based materials, such as C_{60} and [6,6]-phenyl-C_{61}-butyric acid methyl ester, being among the widely used ETLs due to their suitable energy levels, low recombination energy, high electron affinity and mobility, and solution processability.[3,4] Their chemical structure also allows for molecular engineering to tune interfacial properties and improve compatibility with

* *Correspondence to: CFO Graeff, São Paulo State University (UNESP), School of Sciences, Department of Physics and Meteorology, Bauru/SP, Brazil. E-mail: carlos.graeff@unesp.br; or RC Hiorns, CNRS/Univ Pau & Pays Adour, Institut des Science Analytiques et Physico-Chimie pour l'Environnement et les Materiaux, 64053 Pau, Nouvelle-Aquitaine, France. E-mail: roger-clive.hiorns@cnrs.fr*

a *Department of Physics and Meteorology, São Paulo State University (UNESP), School of Sciences, Bauru/SP, Brazil*

b *São Paulo State University (UNESP), School of Technology and Sciences, Presidente Prudente/SP, Brazil*

c *CNRS/Univ Pau & Pays Adour, Institut des Science Analytiques et Physico-Chimie pour l'Environnement et les Materiaux, Pau, France*

d *Department of Chemistry, São Paulo State University (UNESP), School of Sciences, Bauru/SP, Brazil*

perovskite layers.[3,4] Despite their advantages, they suffer from poor solubility in most organic solvents, posing significant challenges for scalable device fabrication.[4] Additionally, the long-term stability of fullerene ETLs and their influence on photovoltaic parameters remain important areas of investigation.

In response to these challenges, main-chain poly(fullerene)s have recently garnered considerable attention due to their unique physicochemical properties.[5] These macromolecular systems have demonstrated notable efficacy as functional additives for improving the operational stability and power conversion efficiency of organic photovoltaic devices,[6] as well as serving as efficient electron-accepting interlayers in PSCs.[7]

A key strategy to address the solubility limitations of fullerene-based materials involves designing alternating copolymers that include comonomers which improve solubilities, such as alkyl- or oligoether-substituted units. These solubilizing segments effectively disrupt the strong intermolecular interactions and aggregation tendencies of fullerene moieties. This, coupled with the linear quality of polymeric chains, enables the formation of high-quality thin films via solution processing. Among the notable advances in this field are synthetic methodologies such as atom transfer radical addition polymerization (ATRAP),[8–10] sterically controlled azomethine ylide cycloaddition polymerization,[11–13] benzyl-azide polymerization[14] and iodine-mediated polymerization (IMP),[15] which have significantly expanded the structural diversity and solubility of main-chain poly(fullerene)s.

In the present paper, we focus on the application of poly{fullerene-*alt*-[1,4-dimethylene-2,5-bis(oxydodecylether)benzene]} ($PC_{60}DB$; Fig. 1). $PC_{60}DB$ was synthesized by both ATRAP and IMP methodologies to give $PC_{60}DB_{(ATRAP)}$ and its IMP variant $PC_{60}DB_{(IMP)}$, respectively. Note that $PC_{60}DB_{(ATRAP)}$ has also been called HSS-12,[10] but here it is denoted $PC_{60}DB_{(ATRAP)}$ to facilitate reading and comparison. Due to the radical nature of both ATRAP and IMP reactions and the large comonomers, both polymers show relatively well-defined structures. In both cases, a single hexagonal ring of the C_{60} cage is disrupted via a 1,4-radical addition of comonomers, although occasionally the second addition can occur on an adjacent hexagon.[8,15] The large side-chains exclude multiple reactions occurring around the C_{60} moieties to ensure a linear chain, and also bestow an exceptional solubility. The PCDBs can readily dissolve even in solvents typically incompatible with C_{60}, such as tetrahydrofuran.

The $PC_{60}DB_{(IMP)}$ (68% yield) and $PC_{60}DB_{(ATRAP)}$ (87% yield) polymers showed respective number-average molar masses (M_n) estimated by steric exclusion chromatography of 19.25 and 11.34 kg mol^{-1}, and dispersities ($Đ = M_w/M_n$) of 1.88 and 1.51 (Figs S1 and S2). The NMR profiles (Figs S3 and S4) are consistent with those reported in our reference article, where $PC_{60}DB_{(IMP)}$ was used in a photovoltaic device.[15]

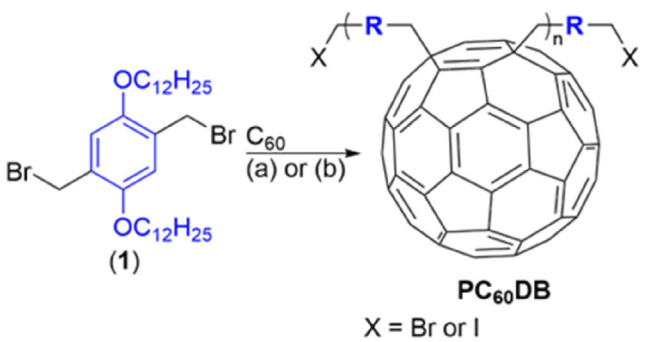

Figure 1. Polymerization scheme. $PC_{60}DB_{(IMP)}$: (a) 18-crown-6 ether, KI, toluene, 140 °C, 22 h; X = I. $PC_{60}DB_{(ATRAP)}$: (b) 2,2′-bipyridine, CuBr, toluene, 140 °C, 22 h; X = Br.

Building on this synthetic foundation, our present study investigated an overlooked aspect of ETL material performance: the effect of polymer aging before device fabrication. While much research has focused on the operational degradation of PSCs, less is known about how storage-related changes in the transport materials themselves can impact device efficiency and stability. Therefore, we aim to shed light on how chemical structure influences long-term processability and interfacial behavior in PSCs by comparing the performance of $PC_{60}DB_{(IMP)}$ and $PC_{60}DB_{(ATRAP)}$ polymers that were stored in a nitrogen-filled glovebox in the dark and at room temperature in three different aging conditions: fresh (*ca* 20 days old), mid-aged (*ca* 6 months old) and aged (*ca* 11 months old) prior to integration in the PSC as ETLs. To be doubly clear, we are not testing the aging of a whole cell, but rather the impact of polymer aging on device efficiency as made. A controlled environment was used to exclude the presence of moisture and oxygen, allowing us to isolate material-intrinsic degradation phenomena.

RESULTS AND DISCUSSION

Figure 2(a),(b) shows the current density–voltage (*J*–*V*) characteristics of the devices, following use of differently aged polymers, in both forward and reverse scanning directions. In Fig. 2(a), PSC incorporating $PC_{60}DB_{(IMP)}$ shows an apparent and gradual decline in photovoltaic performance with the variant fresh and aged polymers. The device with fresh polymer (green curve) behaves almost like an ideal solar cell, with high current output and minimal hysteresis between forward and reverse scans. In the mid-aged state (yellow curve), both short-circuit current density (J_{SC}) and fill factor (FF) drop noticeably, and the curve becomes less rectangular. This decline becomes even more pronounced with the aged polymer (red curve), which results in devices with low current, a distorted *J*–*V* behavior and signs of significant hysteresis. These results indicate that the $PC_{60}DB_{(IMP)}$ polymer loses its ability to form an efficient electron-transporting interface when stored for long periods, even under an inert atmosphere.

In contrast, Fig. 2(b) shows that devices based on $PC_{60}DB_{(ATRAP)}$ maintain relatively stable *J*–*V* characteristics with aging. Since the purpose of this comparison is to evaluate the effects of aging, the fresh $PC_{60}DB_{(IMP)}$ device was used as a reference for both polymer systems. Although performance degrades with time, the transition is less dramatic. Indeed, the *J*–*V* curves for mid-aged and aged $PC_{60}DB_{(ATRAP)}$ retain their shape, and J_{SC} and FF decrease gradually rather than sharply. The open-circuit voltage (V_{OC}) shows smaller changes over time compared to devices with $PC_{60}DB_{(IMP)}$ under forward scanning. Interestingly, the hysteresis appears to be reduced in the aged samples, and its direction is reversed. These results suggest that the polymer may undergo some slow reorganization over time that leads to improved interfacial contact or fewer trap states.

These patterns are quantitatively presented in Table 1 with the statistical plot in Fig. S5. For $PC_{60}DB_{(IMP)}$, J_{SC} drops from around 26 mA cm^{-2} in the fresh state to just 12 mA cm^{-2} after aging. Power conversion efficiency (PCE) follows the same trend, falling from over 17% to under 5%. The FF and V_{OC} also decrease, reflecting less efficient charge extraction and higher recombination. The hysteresis index (HI), estimated via $\left|\frac{PCE_{Rev}-PCE_{Fwd}}{PCE_{Rev}}\right|$, rises

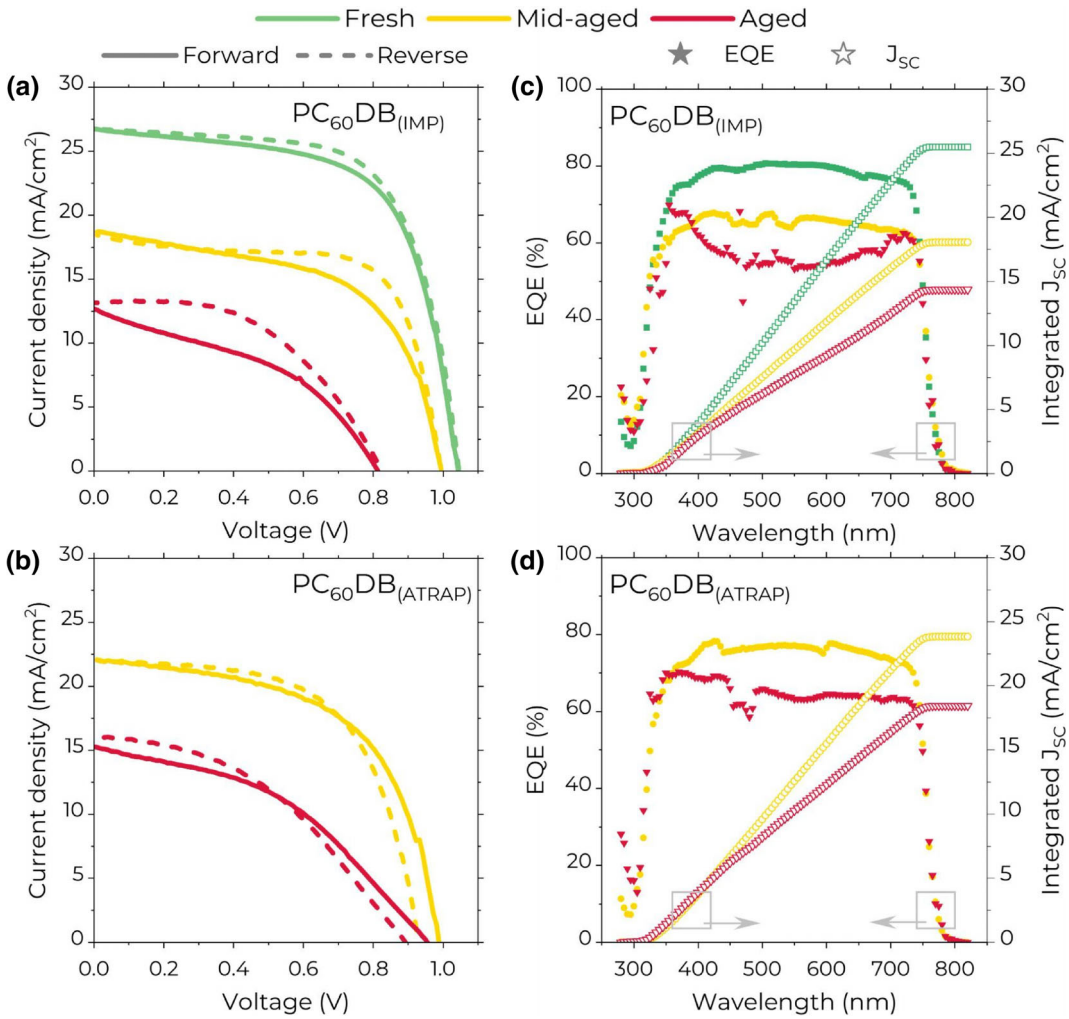

Figure 2. *J–V* characteristics of inverted PSCs using (a) $PC_{60}DB_{(IMP)}$ and (b) $PC_{60}DB_{(ATRAP)}$ as ETL under different aging conditions: fresh (green), mid-aged (yellow) and aged (red). Solid lines represent forward scans, while dashed lines indicate reverse scans. EQE spectra and corresponding integrated J_{SC} for (c) $PC_{60}DB_{(IMP)}$- and (d) $PC_{60}DB_{(ATRAP)}$-based devices.

from 0.03 to 0.17 as the devices age, further indicating instability in charge transport or extraction. On the other hand, $PC_{60}DB_{(ATRAP)}$-based devices show better stability under storage. The PCE decreases from around 12% to about 5.5% mostly due to a moderate reduction in J_{SC} and FF. The HI drops from 0.15 to 0.06.

External quantum efficiency (EQE) spectra and their integrated current curves are exhibited in Fig. 2(c),(d). The integrated current

Table 1. Photovoltaic parameters of inverted PSCs employing PCDB-based ETLs at different aging stages. Data were obtained from forward (Fwd) and reverse (Rev) scans under simulated AM 1.5G illumination. The table reports the open-circuit voltage (V_{OC}), short-circuit current density (J_{SC}), fill factor (FF), power conversion efficiency (PCE) and hysteresis index (HI). For each condition, the best-performing device is highlighted in Fig. S5

Sample	Aging	Scan	V_{OC} (V)	J_{SC} (mA cm^{-2})	FF (%)	PCE (%)	HI
$PC_{60}DB_{(IMP)}$	Fresh	Fwd	1.03 ± 0.01	26.02 ± 1.42	62.21 ± 3.90	16.70 ± 1.42	0.03 ± 0.06
		Rev	1.02 ± 0.04	26.66 ± 1.37	63.67 ± 6.20	17.29 ± 2.18	
	Mid-aged	Fwd	0.96 ± 0.07	18.76 ± 2.44	54.99 ± 9.55	10.17 ± 3.36	0.14 ± 0.10
		Rev	0.94 ± 0.11	19.06 ± 2.31	63.39 ± 7.95	11.71 ± 3.40	
	Aged	Fwd	0.87 ± 0.12	12.22 ± 3.40	37.95 ± 6.00	4.06 ± 1.37	0.17 ± 0.09
		Rev	0.82 ± 0.03	11.95 ± 3.09	50.19 ± 11.94	5.01 ± 1.95	
$PC_{60}DB_{(ATRAP)}$	Mid-aged	Fwd	0.97 ± 0.04	21.26 ± 2.00	56.18 ± 3.19	11.67 ± 1.61	0.15 ± 0.11
		Rev	0.98 ± 0.04	21.55 ± 1.91	64.75 ± 7.24	13.73 ± 2.57	
	Aged	Fwd	0.92 ± 0.06	15.74 ± 1.86	36.78 ± 5.62	5.40 ± 1.43	0.06 ± 0.08
		Rev	0.85 ± 0.05	16.12 ± 1.62	40.79 ± 4.60	5.62 ± 1.23	

densities show good agreement with the J_{SC} values obtained from the *J–V* measurements. Notably, the EQE spectra of the devices exhibit pronounced variation as a function of polymer aging.

The fresh PSC displays a high EQE reaching *ca* 80%, indicating efficient photogenerated charge collection at short-circuit conditions. In contrast, the diminished EQE observed in the mid-aged and aged ones suggests reduced electron extraction and higher recombination at the perovskite (PVK)/ETL interface, which is compatible with the relatively low FF.[16]

The $PC_{60}DB_{(IMP)}$-based EQE spectra show a significant reduction in intensity predominantly within the central visible range (400–650 nm), Fig. 2(c) (red curve), suggesting aging-induced deterioration of charge collection. In contrast, although $PC_{60}DB_{(ATRAP)}$-based devices exhibit an overall decrease in EQE with polymer aging, the drop is less pronounced at around 350 nm, indicating retained charge collection at higher energies.

Despite pronounced variations in the EQE magnitude and spectral profiles, the extracted photovoltaic band gap (E_g^{PV}) remains centered around 1.64 eV (Fig. S6), which is consistent with the expected value for the PVK composition used.[17,18] Furthermore, the aging process induced only a minor shift of less than 10 meV in the respective E_g^{PV} values. Therefore, the changes in device performance after storage of the ETL materials cannot be explained by degradation or stoichiometric alterations of the PVK layer.

Since the $PC_{60}DB$-based polymers were aged independently in the solid state under an inert atmosphere and in the dark, and both the PVK and the polymers were freshly processed for each device, the observed trends must originate from inherent changes within the polymer itself and how these changes impact interfacial interactions upon integration.

In particular, devices incorporating the iodine-terminated polymer ($PC_{60}DB_{(IMP)}$) show a clear decline in efficiency and increased hysteresis with aging. This trend may be related to slow chemical transformations in the carbon–iodine terminal bond, which is known to be relatively weak and highly polarizable.[19] Over time, such bonds may undergo cleavage, internal rearrangement or even promote crosslinking between polymer chains. These subtle molecular changes, although occurring in the solid state, could impact how the polymer interacts with the PVK surface upon device fabrication. Once in contact with the PVK, the polymer may increase the density of interfacial trap states, forming local barriers that hinder charge extraction and promote recombination.[20,21] Additionally, the possible aggregation of excess C_{60} domains in iodine-functionalized ETLs may exacerbate charge trapping and hinder charge extraction.[22]

On the other hand, devices based on the bromine-terminated analogue ($PC_{60}DB_{(ATRAP)}$) exhibit a more stable performance and a reduced hysteresis after aging. The stronger and less polarizable carbon–bromine bond[19] is more resistant to degradation under storage, and its presence may contribute to a more stable interface by passivating interfacial iodine vacancies and limiting ion migration. The gradual decrease in hysteresis may also indicate that mild structural reorganization during aging leads to improved interfacial contact.[23]

Although these changes may not be visible at the macroscopic level, they can still interfere with charge movement across the interface, ultimately affecting the photovoltaic efficiency. Taken together, the results show that even relatively small differences in halogen chemistry can have a meaningful impact on interfacial behavior, with bromine termination helping to create a more stable and reliable interface.

These observations point to the significant influence of end-group chemistry on the functional stability of polymeric ETLs. Although both materials share a similar backbone, the difference in halogen termination leads to distinct outcomes after storage. We hypothesize that, due to the very weak carbon–iodine bond, the iodine appears to promote gradual degradation, while bromine helps preserve or even slightly improve the material's interfacial performance characteristics.

To gain deeper insight into these effects, further investigations are being conducted using spectroscopic, morphological and electrical methods. These studies aim to clarify how molecular structure affects film formation, interfacial quality and charge dynamics in PSCs. The results will contribute to the design of more stable and process-compatible ETLs, which is essential for the development of scalable and long-lasting PVK technologies.

CONCLUSION

This study sheds light on the often-overlooked influence of prefabrication aging on polymer-based ETLs in PSCs. Even when stored in inert conditions, subtle differences in polymer structure can lead to distinct degradation pathways. The pronounced instability observed in iodine-terminated $PC_{60}DB_{(IMP)}$, compared to the more stable performance of $PC_{60}DB_{(ATRAP)}$, underscores the importance of halogen termination in maintaining interfacial quality over time. Gaining a deeper understanding of these intrinsic aging processes will be essential for improving the reliability and manufacturability of perovskite solar technologies.

ACKNOWLEDGEMENTS

This study was financed, in part, by the São Paulo Research Foundation (FAPESP), Brazil, grant numbers 2020/12356-8, 2022/10998-8, 2023/01117-0, 2023/12686-6, 2024/02935-1, 2025/00301-8; and by the Brazilian National Council for Scientific and Technological Development (CNPq) grant number 303750/2024-3. JVP is also grateful for the support of the São Paulo State University research office (PROPe) postdoctoral fellowship (05/2024). CFOG is grateful for the support of CNPq under the Instituto Nacional de Ciência e Tecnologia de Nanomateriais para a Vida (NanoVIDA) no. 406079/2022-6 and FINEP (grant: 01.22.0289.00 (0034-21)). MAGBG and RCH received funding from the European Horizon program under grant agreement HORIZON-CL5-2024-D3-01-02-EFFECTOR-101172820. The Article Processing Charge for the publication of this research was funded by the Coordenação de Aperfeiçoamento de Pessoal de Nível Superior - Brasil (CAPES) (ROR identifier: 00x0ma614).

SUPPORTING INFORMATION

Supporting information may be found in the online version of this article.

REFERENCES

1 Dastgeer G, Nisar S, Zulfiqar MW, Eom J, Imran M and Akbar K, *Nano Energy* **132**:110401 (2024). https://doi.org/10.1016/j.nanoen.2024.110401.
2 Ratnesh RK, Kumar R, Singh S, Chandra R and Singh J, *New J Chem* **49**: 6861–6887 (2025). https://doi.org/10.1039/D5NJ00719D.
3 Zhou G, Luo X, Wang Z, Ding C, Guo Y, Ma C *et al.*, *ChemSusChem* **18**: e202401629 (2025). https://doi.org/10.1002/cssc.202401629.
4 Zhang Y, Zhang S, Dai W and Yang S, *J Mater Chem A* **13**:19046–19072 (2025). https://doi.org/10.1039/D5TA02187A.

5 Gomes MAGB, Gomes OP, Bégué D and Hiorns RC, *Polym Int* This issue.
6 Yu H, Wang Y, Zou X, Yin J, Shi X, Li Y *et al.*, *Nat Commun* **14**:2323 (2023). https://doi.org/10.1038/s41467-023-37738-9.
7 Yin J, Shi X, Wang L, Yan H and Chen S, *Angew Chem Int Ed* **61**: e202210610 (2022). https://doi.org/10.1002/anie.202210610.
8 Hiorns RC, Cloutet E, Ibarboure E, Vignau L, Lemaitre N, Guillerez S *et al.*, *Macromolecules* **42**:3549–3558 (2009). https://doi.org/10.1021/ma900279a.
9 Santos Silva H, Ramanitra HH, Bregadiolli BA, Bégué D, Graeff CFO, Dagron-Lartigau C *et al.*, *J Polym Sci A Polym Chem* **55**:1345–1355 (2017). https://doi.org/10.1002/pola.28502.
10 Silva HS, Ramanitra HH, Bregadiolli BA, Tournebize A, Bégué D, Dowland SA *et al.*, *J Polym Sci B Polym Phys* **57**:1434–1452 (2019). https://doi.org/10.1002/polb.24888.
11 Stephen M, Ramanitra HH, Santos Silva H, Dowland S, Bégué D, Genevičius K *et al.*, *Chem Commun* **52**:6107–6110 (2016). https://doi.org/10.1039/C6CC01380E.
12 Ramanitra HH, Santos Silva H, Bregadiolli BA, Khoukh A, Combe CMS, Dowland SA *et al.*, *Macromolecules* **49**:1681–1691 (2016). https://doi.org/10.1021/acs.macromol.5b02793.
13 Stephen M, Dowland S, Gregori A, Ramanitra HH, Santos Silva H, Combe CM *et al.*, *Polym Int* **66**:388–398 (2017). https://doi.org/10.1002/pi.5273.
14 Bregadiolli BA, Ramanitra HH, Ferreira RM, Corcoles L, Gomes MS, Kang L *et al.*, *Polym Int* **66**:1364–1371 (2017). https://doi.org/10.1002/pi.5419.
15 Batagianni E, Doat O, Elissalt N, Moungadji Bouassa DE, Bittencourt JC, Cardoso Goncalves G *et al.*, *Macromolecules* **58**:1686–1704 (2025). https://doi.org/10.1021/acs.macromol.4c02154.
16 Wang Q, Smith JA, Skroblin D, Steele JA, Wolff CM, Caprioglio P *et al.*, *Sol RRL* **4**:2000213 (2020). https://doi.org/10.1002/solr.202000213.
17 Barrier J, Beal RE, Gold-Parker A, Vigil JA, Wolf E, Waquier L *et al.*, *Energy Environ Sci* **14**:6394–6405 (2021). https://doi.org/10.1039/D1EE01184G.
18 Nogueira GL, Lopez-Richard V, Meneghetti JLA, Hartman F and Graeff CFO, *Sol RRL* **9**:e202500562 (2025). https://doi.org/10.1002/solr.202500562.
19 Cavallo G, Metrangolo P, Milani R, Pilati T, Priimagi A, Resnati G *et al.*, *Chem Rev* **116**:2478–2601 (2016). https://doi.org/10.1021/acs.chemrev.5b00484.
20 Wu W-Q, Rudd PN, Ni Z, Van Brackle CH, Wei H, Wang Q *et al.*, *J Am Chem Soc* **142**:3989–3996 (2020). https://doi.org/10.1021/jacs.9b13418.
21 Li Y, Wang Z, Yu P, Chen Y, Wu R, Zhao X *et al.*, *Sol RRL* **9**:2500066 (2025). https://doi.org/10.1002/solr.202500066.
22 Yoon H, Kang SM, Lee J-K and Choi M, *Energy Environ Sci* **9**:2262–2266 (2016). https://doi.org/10.1039/C6EE01037G.
23 Chen Z, Jiang S, Liu Z, Li Y, Shi J, Wu H *et al.*, *J Mater Chem A* **12**:16070–16078 (2024). https://doi.org/10.1039/D4TA01872A.